PHILOSOPHICAL TRANSACTIONS A

rsta.royalsocietypublishing.org

Research

Article submitted to journal

Subject Areas:
chemical physics

Keywords:
Non-adiabatic dynamics; MCTDH; vMCG; Surface hopping; Direct Dynamics

Author for correspondence:
G. A. Worth
e-mail: g.a.worth@ucl.ac.uk

Mixed-Quantum-Classical or Fully-Quantised Dynamics? A Unified Code to Compare Methods

J. Coonjobeeharry[1], K. E. Spinlove[2], C. Sanz Sanz[3], M. Sapunar[4], N. Došlić[4] and G. A. Worth[1]

[1]Department of Chemistry, University College London, 20, Gordon St., London, WC1H 0AJ, U.K.
[2]Faculty of Science and Engineering, University of Groningen, Nijenborgh 4, 9747AG, Groningen, Netherlands
[3]Department of Applied Physical Chemistry. Faculty of Science. Autonoma University Madrid. Campus Cantoblanco. 28049, Madrid, Spain.
[4]Department of Physical Chemistry, Ruđer Bošković Institute, Bijenička 54, 1000 Zagreb

Three methods for non-adiabatic dynamics are compared to highlight their capabilities. Multi-configurational time-dependent Hartree (MCTDH) is a full grid-based solution to the time-dependent Schrödinger equation, variational multi-configurational Gaussian (vMCG) uses a less flexible but unrestricted Gaussian wavepacket basis, and trajectory surface hopping (TSH) which replaces the nuclear wavepacket with a swarm of classical trajectories. Calculations with all methods using a model Hamiltonian were performed. The vMCG and TSH were also then run in a *direct dynamics* mode, with the potential energy surfaces calculated on-the-fly using quantum chemistry calculations. All dynamics calculations used the QUANTICS package, with the TSH calculations using a new interface to a surface hopping code. A novel approach to calculate adiabatic populations from grid-based quantum dynamics using a time-dependent discrete variable representation (TDDVR) is presented, allowing a proper comparison of methods.

THE ROYAL SOCIETY PUBLISHING

1. Introduction

To understand the dynamical behaviour of a molecular system requires a solution to the time-dependent Schrödinger equation (TDSE) for both nuclei and electrons. The large mass difference between nuclei and electrons facilitates a decoupled treatment of their respective dynamics. This is provided by the adiabatic Born-Oppenheimer Approximation (BOA), which has been fundamental to theoretical studies of chemical dynamics. The nuclei of a molecule are considered *clamped*, and the diagonalisation of the electronic Hamiltonian leads to a set of eigenvalues which depend parametrically on the nuclear (slow) coordinates. From this adiabatic potential energy surfaces (PESs) over nuclear space [1] can be formed. These PESs are defined such that the energetic ordering of electronic states is conserved, but in general not their physical character [2].

However, for molecular dynamics initialised on excited electronic states, there are often breakdowns of the BOA due to the finite kinetic energy of the nuclei. By expanding the nuclear kinetic energy operator in the electronic basis, in terms of the scalar and vector derivative couplings with respect to the nuclear coordinates, it can be shown that the first order vector derivative nuclear couplings between adiabatic electronic states are inversely proportional to the energy splittings between the adiabatic PESs. The energy splittings between excited adiabatic PESs are often comparable to, or smaller than, their corresponding non-adiabatic couplings, leading to non-adiabatic transitions between electronic states [3].

Over the past few decades efficient computational methods to solve the time dependent Schrödinger Equation, with the aim of modelling non-adiabatic processes, have been developed to improve our understanding of chemical problems involving excited states. These range from bioluminescence to electron transfer processes, with applications in renewable energy, chemical synthesis, and bioimaging. Two main families of methods have evolved: fully-quantised electron-nuclear dynamics such as Multi-configurational time-dependent Hartree (MCTDH), and mixed-quantum-classical dynamics such as Trajectory Surface Hopping (TSH). MCTDH uses discrete variable representation (DVR) grid basis sets to describe both the Hamiltonian and wavefunction [4]. In TSH, quantum electronic amplitudes are integrated together with classical nuclear trajectories to dictate when nuclear trajectories hop between electronic states [5]. A third family of methods employs Gaussian basis set expansions of the wavepacket built around trajectories that can either be treated classically or quantum mechanically. The variational Multi-configurational Gaussian Method (vMCG) is an example of such an approach. This method includes explicit coupling between Gaussian amplitudes, allowing the Gaussian functions to follow quantum trajectories [6].

Each method takes a different expansion of the wavefunction. This facilitates contrasting treatments of the molecular dynamics under different approximations, each with their own advantages and disadvantages. MCTDH requires high-accuracy pre-calculated PESs and nonadiabatic coupling matrices, limiting its use to comparatively small systems or reduced dimensionality treatments of molecules. To examine molecular dynamics in full configuration space, TSH is a potential solution. As trajectory based approaches allow for the simultaneous calculation of required electronic structure (electronic-state energies and gradients) on-the-fly, alongside the nuclear dynamics. However, TSH cannot be derived from first principles, and a classical propagation of nuclear motion may fail to explain experimentally observed behaviour [7].

In contrast, vMCG can be derived from first principles, and converges on the exact solution in well-defined limits. Additionally, as for TSH, the travelling nature of Gaussian basis functions facilitates *direct dynamics*, with 'on-the-fly' calculations of electronic structure quantities via an interface between the quantum-dynamics and quantum-chemistry programs. The direct dynamics variant of vMCG is known as Direct-dynamics variational Multi-configurational Gaussian (DD-vMCG).

The aim of this paper is to compare a fully-quantised dynamics method (MCTDH) with an approximate quantised method (vMCG/DD-vMCG) and a mixed quantum-classical method

(TSH/DD-TSH) which utilises Tully's 'fewest switches' algorithm to determine the probability that nuclear trajectories hop between electronic states [8]. The main question that this paper addresses is how well vMCG and TSH converge: how many nuclear trajectories are required, and how do the converged mixed-quantum classical dynamics compare with analogous fully-quantised dynamics calculated for the same systems? All calculations have been made using the same code to ensure identical initial conditions and potential surfaces. For this we use the QUANTICS package to provide a unified code [9,10], which has been interfaced to an independent surface hopping code. A major difficulty for the comparison of full quantum and surface hopping calculations is that the former are run in the diabatic picture, while the latter are in the adiabatic picture. Transforming between them is difficult due to the global nature of the adiabatic-diabatic transformation operator. Here we present the use of a time-dependent discrete variable representation to efficiently evaluate this operator for large quantum dynamics calculations.

Two systems are used in the comparison: the butatriene cation, and cyclohexadiene ring-opening. The butatriene cation is a classic molecule in non-adiabatic theory. It features a strongly peaked conical intersection between the first two states that gives a strong signal of non-adiabatic coupling in the photo-electron spectrum [11]. Model potentials are available [12] and it has also been used in DD-vMCG tests [13]. The ring opening in cyclohexadiene, leading to hexatriene, is an important motif in photochemistry [14]. It presents a more challenging test as three electronic states joined by sloped intersections are involved in the passage of the initially excited wavepacket to the ring-opened form. Cyclohexadiene has also been the subject of a number of theoretical and experimental studies [15].

Both of these molecules, with 18 and 36 internal degrees of freedom respectively, are large for quantum dynamics simulations. Cyclohexadiene, in particular, is at the edge of what can be reasonably treated both by the nuclear dynamics and the electronic structure theory required for the potential surfaces. The results show that there is good agreement using all three methods for butatriene, and this size and type of system is now relatively straightforward for simulations. For cyclohexadiene, it is not possible to obtain converged results, but the similarities between the dynamics obtained by the different methods supports these results as qualitatively correct.

2. Background Theory

The three methods to be compared solve the TDSE for a system of distinguishable nuclei

$$i\hbar\frac{\partial}{\partial t}\Psi(\mathbf{q},\mathbf{t}) = \hat{\mathbf{H}}\Psi(\mathbf{q},\mathbf{t}) \tag{2.1}$$

to obtain the time-evolution of the wavefunction $\Psi(t)$ for a given Hamiltonian, $\hat{H}$ and set of initial conditions $\Psi(0)$. All three are well-documented elsewhere and only an overview will be given here to provide a comparison of their characteristics. Further details can be found in the literature for MCTDH [4,16], vMCG [6,17] and TSH [18,19].

(a) The Multi-Configurational Time-Dependent Hartree Method (MCTDH)

In MCTDH, the nuclear wavefuction is expanded in a set of configurations

$$\Psi(\mathbf{q},t) = \sum_J A_J(t)\Phi_J(\mathbf{q},t) \tag{2.2}$$

These configurations are expanded in a direct-product basis of time-dependent functions known as *single-particle functions* (SPFs)

$$\Psi(\mathbf{q},t) = \sum_{j_1=1}^{n_1}\cdots\sum_{j_p=1}^{n_p} A_{j_1\ldots j_f}(t)\prod_{\kappa=1}^{p}\varphi_{j_\kappa}^{(\kappa)}(Q_\kappa,t) \tag{2.3}$$

which in turn are expanded using time-independent functions, known as the *primitive basis*

$$\varphi_j^{(\kappa)}(Q_\kappa,t)=\sum_{k=1}^{N_\kappa^d} a_{kj}^{(\kappa)}(t)\chi_k^{(\kappa)}(Q_\kappa) \tag{2.4}$$

Note that the SPFs can be multi-dimensional, i.e. the particle coordinate Q^κ can be a number of system coordinates q. For this reason the underlying grid formed by the time-independent basis set can be multi-dimensional, represented by the summation limit of N^d where N is the number of grid functions and d the dimensionality of the SPF.

The TDSE is solved by propagating the SPFs and expansion coefficients using equations of motion that are obtained from the Dirac-Frenkel variational principle [20].

$$i\dot{A}_J = \sum_L \langle \Phi_J|H|\Phi_L\rangle A_L \tag{2.5}$$

$$i\dot{\varphi}^{(\kappa)} = \left(1-P^{(\kappa)}\right)\left(\rho^{(\kappa)}\right)^{-1}\langle \mathbf{H}\rangle^{(\kappa)}\varphi^{(\kappa)} \tag{2.6}$$

Here, $\langle \mathbf{H}\rangle^{(\kappa)}$ is a mean-field operator coupling the motion of the "particles", $\rho^{(\kappa)}$ is a reduced density matrix for the particle and $P^{(\kappa)}$ is a projector onto the space spanned by the SPFs.

The memory requirements of MCTDH are dominated by the wavefunction. This can be written schematically as

$$\text{memory} \propto n^p + pnN^d \tag{2.7}$$

where n is the number of SPFs for the p particles, which in a real calculation will be different for each particle. The first term is the storage required for the expansion coefficients and the second for the SPFs. The effort is mostly due to the need to build the mean-fields at each step, which requires

$$\text{effort} \propto rp^2n^{(p+1)} \tag{2.8}$$

where r is the number of terms in the Hamiltonian. The number of coefficients and effort exhibits the exponential growth with system size that provides the major bottleneck for all numerically exact solutions to the TDSE. The power of MCTDH comes from balancing this growth with the memory and effort required to propagate the SPFs, allowing much larger systems to be treated than grid-based methods expanded directly in terms of the time-independent primitive basis.

The MCTDH method can be thought of as a tensor contraction scheme, reducing the representation on a multi-dimensional grid to an expansion in low-dimensional functions. For even larger systems this contraction can be increased by using a multi-layer scheme in which the SPFs are expanded in layers of multi-dimensional functions using the MCTDH form [21,22]. This has been used to treat wavefunctions with more than 1000 degrees of freedom.

The main restriction of the MCTDH method is the requirement for a global potential that must be known before the propagation takes place. For efficiency the potential must also be in the form of a sum of products of low-dimensional operators to allow easy evaluation of the matrix elements required to build the mean-fields and Hamiltonian. The building of a suitable model Hamiltonian thus requires the careful choice of coordinates and functional form for the potential for an accurate representation of a system. This may restrict the dynamics that can be simulated, for example low-order polynomial fits may not include the coupling or potential forms for long-range motions and long time-scales.

(b) The variational Multi-Configurational Gaussian Method (vMCG)

If one or more of the grid-based SPFs of the MCTDH ansatz, Eq. (2.3), are replaced with parameterised Gaussian functions, the G-MCTDH method is obtained [23]. The equations of

motion for the parameters of the multi-dimensional Gaussian basis functions (GBFs),

$$g_j(\mathbf{Q},t) = \exp\left(\mathbf{Q}^T\boldsymbol{\zeta}_j\mathbf{Q} + \mathbf{Q}^T\boldsymbol{\xi}_j + \eta_j\right) \tag{2.9}$$

are also obtained using the Dirac-Frenkel variational principle. When all basis functions are replaced by GBFs, the vMCG wavefunction is obtained, a simple superposition of GBFs.

$$\Psi(\mathbf{q},t) = \sum_j A_j g_j(\mathbf{q},t) \tag{2.10}$$

The equations of motion for the vMCG method can be written

$$\begin{aligned} i\dot{A}_j &= \sum_{lk} \mathcal{S}^{-1}_{jk}\langle g_k|H|g_l\rangle A_l - \sum_{\kappa=1}^{p}\sum_{l=1}^{n_\kappa} iS^{-1}_{jk}\langle g_k|\frac{\partial}{\partial t}g_l\rangle A_{J_l^\kappa} \\ i\dot{\boldsymbol{\Lambda}} &= \mathbf{C}^{-1}\mathbf{Y} \end{aligned} \tag{2.11}$$

where $\mathbf{S}$ is the GBF overlap matrix, $\boldsymbol{\Lambda}$ is a vector containing the GBF parameters, while $\mathbf{C}$ and $\mathbf{Y}$ contain GBF matrix elements of Gaussian moments and the Hamiltonian respectively.

The GBFs can also be written in the form of Gaussian Wavepackets (GWPs) [24]

$$g(\mathbf{q},t) = \exp[-(\mathbf{q}-\mathbf{q_0})^{\mathrm{T}}\boldsymbol{\alpha}(\mathbf{q}-\mathbf{q_0}) + i\mathbf{p_0}^{\mathrm{T}}(\mathbf{q}-\mathbf{q_0}) + i\gamma] \tag{2.12}$$

where α is the width, γ the phase, and q_0, p_0 the position and momentum of the centre of the GWP. It can then be shown that the center of the basis functions, that will be referred to as GWPs in the following, follow a trajectory that has a "quantum coupling" in addition to the classical trajectory [6]. Other methods that use GWPs as a basis to solve the TDSE, such as multiple spawning [25,26] and coherent coupled states [27] allow the basis functions to follow just the classical trajectory. The equivalence of the approaches has been shown [28]. In vMCG, for stability and simplicity, the width parameter is kept fixed and *frozen* GWPs are used.

The first advantage of vMCG over MCTDH is that the small parameter set makes for a very compact wavefunction. For simplicity and stability, the GWPs are taken to be separable with time-independent widths. The memory required for a wavefunction is then

$$\text{memory} \propto n + fn \tag{2.13}$$

The number of coefficients is given by the number of configurations, n, and each GWP requires one complex number per degree of freedom ($\lambda_{aj} = -2\alpha_j q_{0,aj} + ip_{0,aj}$) as the phase can be incorporated into the expansion coefficient. The effort has 2 main terms

$$\text{effort} \propto (fn)^3 + nf^3 \tag{2.14}$$

where the first term is due to the inversion of the $\mathbf{C}$ matrix, and the second term is due to the integrals that need to be calculated, assuming the potential surfaces are represented by a local harmonic approximation (LHA) [6].

In MCTDH, the reduced density matrices give a measure of how close to convergence a calculation is as they can be related to the importance of the basis functions. Unfortunately with vMCG there is no way of knowing how many configurations are required for convergence: one simply has to add more functions until the property of interest no longer changes. In comparison to other GWP (or trajectory) based methods, the variational nature of vMCG does guarantee that adding more functions will improve the result, and it will converge as fast as possible. It also means that, as in MCTDH, as long as the initial conditions are satisfied, placement of the initial GWPs does not affect the final result.

For large systems, while the memory requirements remain small, the effort unfortunately quickly becomes large. To alleviate this it is possible to break the problem into smaller parts. Returning to the original MCTDH ansatz, instead of replacing the SPFs by GWPs, it is more fruitful to consider the GWPs as a time-dependent primitive basis set and expand the SPFs in terms of these [6]. This leads naturally to a multi-layer version able to treat many degrees of

freedom [29,30]. In the present work, however, we will stick to the single layer ansatz Eq. (2.3) and expand the SPFs

$$\varphi_j^{(\kappa)}(Q_\kappa) = \sum_{k=1}^{N_\kappa^d} a_{kj}^{(\kappa)}(t) g_k^{(\kappa)}(Q_\kappa, t) \tag{2.15}$$

If the GWPs are frozen and separable, it can be easily shown that this approach still uses a superposition of GWPs for the wavefunction ansatz

$$\begin{aligned} \Psi(\mathbf{q},t) &= \sum_{j_1=1}^{n_1} \cdots \sum_{j_p=1}^{n_p} A_{j_1 \ldots j_f}(t) \prod_{\kappa=1}^{p} \left(\sum_{k_\kappa=1}^{N_\kappa^d} a_{k_\kappa j_\kappa}^{(\kappa)}(t) g_{k_\kappa}^{(\kappa)}(Q_\kappa, t) \right) \\ &= \sum_{k_1=1}^{N_1} \cdots \sum_{k_p=1}^{N_p} B_{k_1 \ldots k_f}(t) \prod_{\kappa=1}^{p} g_{k_\kappa}^{(\kappa)}(Q_\kappa, t) \end{aligned}$$

with a basis set of N^p multi-dimensional GWPs. Here, however, they are now correlated at the particle level, i.e. due to interaction between the particles, whereas in vMCG all the GWPs are correlated only at the configuration level, i.e. by the motion of the different configurations.

If the number of GWPs for each particle is the same as the number of SPFs used (i.e. $N = n$), then the equations of motion are

$$\begin{aligned} i\dot{A}_J &= \sum_L \langle \Phi_J | H | \Phi_L \rangle A_L \\ i\dot{a}_{kj} &= -\sum_{lm} S_{kl}^{-1} \tau_{lm} a_{mj} \\ i\dot{\boldsymbol{\Lambda}}_k &= \mathbf{C}_k^{-1} \mathbf{Y}_k \end{aligned} \tag{2.16}$$

The wavefunction expansion coefficients are now an orthonormal vector, which improves stability over the original vMCG equations of motion, and the SPF coefficients evolve due to the GWP motion. The equations of motion for the GWPs have the same form as before, but now the $\mathbf{Y}$ vector contains mean-field terms coupling the GWPs in different particles. The full form of the terms is given in the literature [29,30]. The Hamiltonian now has to be written in a form that is separable between the particles. This is straightforward for a vibronic coupling model that is a polynomial expansion, but the Shepard interpolated potentials used in DD-vMCG must be reformulated with a separate polynomial expansion for each configuration. This leads to a large number of terms in the Hamiltonian.

In the following, to emphasize the connection to vMCG, this approach will be termed *multi-mode* vMCG (MMvMCG) rather than the formally correct name of 1-ML-GMCTDH. By introducing this effective partitioning of the vMCG basis functions, the memory requirements for the wavefunction are increased to

$$\text{memory} \propto n^p + nf \tag{2.17}$$

due to the number of configurations. Concurrently the effort becomes

$$\text{effort} \propto rp^2 n^{(p+1)} + \left(\frac{f}{p} n\right)^3 + n \left(\frac{f}{p}\right)^3 \tag{2.18}$$

Here, the first term is due to the re-introduction of mean-fields (r is again the number of terms in the Hamiltonian), while the other terms are reduced from the vMCG effort due to the smaller number of degrees of freedom in each set of GWPs ($\frac{f}{p}$). As always with MCTDH based methods, a play off between number of configurations against size of particles is required for optimum efficiency.

(c) Trajectory Surface Hopping

The classical trajectory surface hopping method is based on a mean-field separation of classical and quantum motions, as adopted in the Ehrenfest method. Nuclei are treated by a classical discretisation of the nuclear wavepacket. The electronic Hamiltonian matrix is then separated, leading to coupled partial differential equations for the electronic state amplitudes which can be used to derive a "hopping probability" for a molecule along a trajectory to change electronic state. [5]

Firstly, the total wavefunction is expanded as a sum over electronic states:

$$\Psi\left(r,R,t\right)=\sum_{i}\Phi_{i}\left(r,R\right)\Omega_{i}\left(R,t\right) \tag{2.19}$$

This multiconfiguration expansion ensures that every electronic quantum state i is described by a different nuclear wavefunction $\Omega_i\left(R,t\right)$. The electronic basis functions $\Phi_i\left(r,R\right)$ are assumed to be orthonormal, whilst the nuclear basis functions are not; the integral over R of $|\,\Omega_i\left(R,t\right)|^2$ gives the population of state i at time t.

By substituting equation 2.19 into the TDSE, premultiplying by $\Phi_j^*\left(R,t\right)$ and integrating over the electronic coordinates, coupled differential equations for the time evolution of the nuclear basis functions are obtained:

$$i\hbar\frac{\partial\Omega_{j}}{\partial t}=-\frac{\hbar^{2}}{2}\sum_{\alpha}M_{\alpha}^{-1}\nabla_{R_{\alpha}}^{2}\Omega_{j}+\sum_{i}H_{ji}\Omega_{i}-\frac{\hbar^{2}}{2}\sum_{\alpha,i}M_{\alpha}^{-1}D_{ji}^{\alpha}\Omega_{i}-\hbar^{2}\sum_{\alpha,i\neq j}M_{\alpha}^{-1}d_{ji}^{\alpha}\nabla_{R_{\alpha}}\Omega_{i} \tag{2.20}$$

where $d_{ji}^{\alpha}=\int\Phi_{j}\nabla_{R_{\alpha}}\Phi_{i}dr$ and $D_{ji}^{\alpha}=\int\Phi_{j}\nabla_{R_{\alpha}}^{2}\Phi_{i}dr$ are the first and the second order nonadiabatic coupling elements.

By substituting the phase formulation of the nuclear wavepacket [31]

$$\Omega_{j}\left(R,t\right)=A_{j}\left(R,t\right)\exp\left(\frac{i}{\hbar}S_{j}\left(R,t\right)\right) \tag{2.21}$$

into Equation 2.20, separating imaginary and real terms (under the premise that the amplitude, $A_j\left(R,t\right)$, and phase, $S_j\left(R,t\right)$, are real-valued), "creative" partitioning of the diagonal and off-diagonal electronic Hamiltonian matrix, and taking a classical limit $\hbar=0$, equations 2.22 and 2.24 are obtained.

The first is an equation describing nuclear motion on electronic PES H_{jj}:

$$\frac{\partial S_{j}}{\partial t}+\sum_{\alpha}\frac{1}{2}M_{\alpha}^{-1}\left(\nabla_{R_{\alpha}}S_{j}\right)^{2}+H_{jj}=0 \tag{2.22}$$

Equation 2.22 closely resembles the classical Hamilton-Jacobi Equation if $S_i\left(t\right)$ is defined as the classical action and its derivative related to the nuclear momentum

$$S_{i}\left(t\right)=\int_{0}^{t}L_{i}(t')dt'\quad;\quad\frac{\partial R_{i}}{\partial t}=M_{\alpha,i}^{-1}\nabla_{R_{\alpha}}S_{j} \tag{2.23}$$

The second equation describes the transport of flux between PESs governed by the non-adiabatic coupling vector d_{ij}^{α}, and off-diagonal terms of the electronic Hamiltonian H_{ij}.

$$\begin{aligned}&\frac{\partial A_{j}}{\partial t}+\sum_{\alpha}M_{\alpha}^{-1}\nabla_{R_{\alpha}}A_{j}\nabla_{R_{\alpha}}S_{j}+\sum_{\alpha}\frac{1}{2}M_{\alpha}^{-1}A_{j}\nabla_{R_{\alpha}}^{2}S_{j}+\\&\sum_{i\neq j}A_{i}\left(\left(\sum_{\alpha}\frac{\partial R_{i,\alpha}}{\partial t}d_{ji}^{\alpha}+\frac{i}{\hbar}H_{ji}\right)\exp\left(-\frac{i}{\hbar}\int_{0}^{t}\left(H_{ii}-H_{jj}\right)dt'\right)\right)=0\end{aligned} \tag{2.24}$$

In TSH, the nuclear wavefunctions are discretised into a set of particle-like trajectories, represented by phase space points that are propagated over electronic potential energy surfaces. Since in the trajectory picture each distinct, classical, phase space point is defined universally over

all electronic quantum states and the same nuclear kinetic energy is associated with all electronic quantum states. Accordingly, it can be shown that

$$\exp\left(-\frac{i}{\hbar}\int\left(H_{ii}-H_{jj}\right)dt\right)=\exp\left(\frac{i}{\hbar}\left(S_i-S_j\right)\right) \tag{2.25}$$

Therefore, Equation 2.24 is analogous to Liouville's classical diffusion equation governing the continuity of nuclear flux in phase space. The amplitude of the nuclear functions $\Omega_j\left(R,t\right)$, $A_i\left(R,t\right)$ can be identified with time dependent basis function amplitudes for the electronic wavepacket in Ehrenfest's Classical Mean Field approach. These electronic basis functions can either be in the adiabatic or diabatic representation (as long as they are orthonormal). However, TSH typically employs the adiabatic electronic representation, because in the adiabatic representation, off diagonal terms in the electronic Hamiltonian, $H_{ij}=0$, justifying the partitioning described to obtain equations 2.22 and 2.24.

In this way, hopping of the nuclear trajectories between electronic PESs is governed by the electronic expansion coefficients. However, the coupling terms in equation 2.24 make direct solutions for the electronic populations difficult to obtain when the nuclear wavepacket is discretised. The "fewest switches" algorithm (FS) maintains correct electronic state populations by a variational solution of equation 2.24 that minimises the number of hops of the nuclear trajectories between electronic PESs. FS uses a stocastic approach to branch nuclear trajectories in a way that achieves the correct statistical distribution of electronic state populations. For a two-electronic-state model, such as the butatriene cation, the probability of a hop from state 1 to state 2 during incremental timestep Δt is given by

$$P_{1\rightarrow2}=-\frac{d(\log|A_1\left(t\right)|^2)}{dt} \tag{2.26}$$

If $P_{1\rightarrow2}<0$ then no hop occurs. A major deficiency of this hopping algorithm is that occasionally, non-zero probabilites are determined for trajectory hops that are forbidden by classical energy conservation.

The big advantage of TSH is that the system is being modelled by a set of independent classical trajectories and the effort for one of these scales linearly with the number of degrees of freedom. However, the stochastic nature of the method means that many trajectories may be needed for a converged result, and the approximations made mean that it is not guaranteed to converge on the solution to the TDSE. For example, when the nuclei are able to visit multiple distinct regions of high derivative coupling, off-diagonal quantum density matrix elements of individual trajectories can become much larger than the exact quantum coherence. This leads to unwarranted trajectory hopping between adiabatic PESs. To overcome this, a range of decoherence corrections have been proposed [19,32–34], including one recently derived from an exact factorisation of the molecular wavefunction [35].

Over-coherence can be exacerbated by the way the momentum is rescaled after a trajectory hops between adiabatic electronic PESs. The difference in electronic potential energy between states at the transition point is accommodated by an *ad hoc* rescaling of the nuclear momentum in strict accordance with classical energy conservation. However, rescaling the nuclear momentum for this purpose has no rigorous foundation based on first principles [36], and the manner in which it is done is non-unique and is a subject of debate. Two common methods are isotropic velocity rescaling, and rescaling solely along the non-adiabatic coupling vector (NACV) [35]. Whilst rescaling along the NACV is believed to be more justified theoretically from semi-classical arguments [37–39], both approaches have been recently shown to violate the principle of conservation of angular momentum [40]. In addition, NACV momentum rescaling means only kinetic energy along the NACV is available, and this can result in poorer internal consistency. For instance, NACV momentum rescaling generally results in more rejected (known as "frustrated") hops, where the classical nuclear trajectory does not have enough kinetic energy to surmount the energy barrier presented by the difference in potential energy between adiabatic electronic states.

3. Computational Methods

All dynamics calculations were made using the QUANTICS Package [9,10]. Both MCTDH and vMCG are part of the core implementation of the code. The surface hopping calculations used an interface between QUANTICS and a general surface hopping code written by Sapunar and Došlić [41], referred to here as ZAGREB SH. The QUANTICS code is able to generate a range of initial wavefunctions and links to a number of potential routines that can be input as text files for analytical functions, such as the vibronic coupling Hamiltonian used here. The QUANTICS-Zagreb SH interface means that the MCTDH, vMCG and TSH calculations can be started with identical starting conditions and use the same potential surfaces.

The TSH calculations used the classic "fewest switches" algorithm [8], along with the decoherence correction of Granucci and Persico [34]. A time-step of 0.1 fs was used. Hopping probabilities have been computed from analytically obtained nonadiabatic couplings and isotropic velocity scaling is used to conserve energy. While it was not needed here, in cases when the non-adiabatic couplings are not available or cannot be computed with sufficiently small time steps due to the cost of the underlying electronic structure calculation, it is advantageous to evaluate the hopping probabilities from overlaps of wave functions computed at each step of the nuclear dynamics. This can be done either in the adiabatic basis using, for instance, norm preserving interpolation [42,43] or in the locally diabatic basis [44,45]. For comparison of these methods see Xie *et al.* [41,45].

QUANTICS has an interface to a range of quantum chemistry codes to generate surfaces during on-the-fly calculations. Surfaces are stored as points in a Quantum Chemistry (QC) database. Full details of how the QC database is generated are given in Refs. [6,46]. In brief, points are added to the database when the centre of a GWP (or point on a trajectory) is further than a specified distance from any point in the database. A QC calculation provides the energies, gradients and derivative couplings at this point, and the Hessians are obtained using a Hessian updating scheme. The potential surfaces used in the propagation are then obtained using Shepard interpolation between the points in the database.

For DD-vMCG, the surfaces must be in the diabatic picture, and this representation is also better for the Shepard interpolation as the surfaces are smoother. The QC data is transformed to the diabatic picture using a global diabatisation scheme [13], in which the adiabatic-diabatic transformation matrix is propagated using the calculated derivative couplings. This scheme has been shown to provide globally consistent surfaces for a 2-state system [46]. The QC database can also be either generated or used by either DD-TSH or DD-vMCG calculations. For DD-TSH, the surfaces used are the adiabatic potentials and derivative couplings obtained from the interpolated surfaces.

The calculations here model a vertical excitation from the vibronic ground-state wavefunction in the harmonic approximation. All calculations were run in dimensionless (mass-frequency scaled) normal mode coordinates. As Zagreb SH runs Newtonian trajectories in Cartesian coordinates, QUANTICS made the required coordinate transformation. In the coordinates used, the initial wavepacket is a separable Gaussian function with a width of $\frac{1}{\sqrt{2}}$ along each coordinate. The GWP basis functions for the vMCG calculations have the width of the ground-state function, and the initial wavefunction is an exact representation with only one function populated. All GWPs have the same initial coordinate, the Franck-Condon point, but different momenta. The initial conditions for the TSH calculations were generated using random sampling of the Wigner distribution associated with the ground-state wavefunction. The sampling retains the symmetry of the distribution by always adding 4 points for each random selection, one in each quadrant of phase space. At the end of a TSH calculation, QUANTICS combines the data from the trajectories to allow analysis by its suite of analysis programs.

4. The Systems to be Studied

(a) Vibronic Coupling Model: Butatriene Cation

Initial simulations were made using the well-known vibronic coupling model [47,48] for the lowest two states of the butatriene cation. This model system is chosen as a representative but simple example of a two-state, single, peaked conical intersection.

The vibronic coupling model assumes a diabatic basis and makes a Taylor expansion of the potential surfaces and diabatic coupling aroung the Franck-Condon point. For the butatriene cation model used here, the expansion of the diabatic potentials is made to second order, and the couplings to first order. The Hamiltonian matrix can be written

$$\mathbf{H} = \mathbf{H}_0 + \mathbf{W}^{(0)} + \mathbf{W}^{(1)} + \mathbf{W}^{(2)} \tag{4.1}$$

where $\mathbf{H}_0$ is a zero-order Hamiltonian. As the coordinates are the neutral ground-state mass-frequency scaled normal-modes, this is composed of the kinetic energy operator and the neutral ground-state potentials in the harmonic approximation. It is thus diagonal with identical elements:

$$\mathbf{H}_0 = H_0\mathbf{1} \quad ; \quad H_0 = \sum_\alpha \frac{1}{2}\frac{\partial^2}{\partial q_\alpha^2} + \frac{1}{2}\omega_\alpha q_\alpha^2 \tag{4.2}$$

where $\mathbf{1}$ is the unit matrix. The $\mathbf{W}^{(i)}$ matrices add corrections at the different orders of the expansion: $\mathbf{W}^{(0)}$ contains the energies of the states at the Frank-Condon point, $\mathbf{W}^{(1)}$ the linear terms (gradient and non-adiabatic coupling), etc. The parameters for the Taylor expansion terms in the higher order matrices are obtained by fitting to electronic structure calculations and experimental data to reproduce the photo-electron spectrum and are contained in Ref. [12]. This model is able to describe the strongly peaked conical intersection coupling the cation $\tilde{X}$ and $\tilde{A}$ states.

(b) Direct Dynamics: Butatriene and Cyclohexadiene

The electronic ground state of the butatriene cation has B_{2g} symmetry (X^2B_{2g}-state) and the first excited state has B_{2u} symmetry (A^2B_{2u}-state). The electronic structure for these states was treated using a state-averaged complete active space self consistent field (SA-CASSF) wavefunction with 5 electrons in the 6 π orbitals. A small 3-21G* basis set was used for speed. This is known to adequately describe the conical intersection between the two states. All calculations were made using the Gaussian09 program [49].

Cyclohexadiene has two low-lying electronic states: $S_1(^1B_1)$ and $S_2(^1A_1)$ which have $\pi\pi^*$ character. The former is a singly excited state while the latter is a mixture of single and double excitations. The conventional mechanism after photo-excitation to the bright S_1 state is a fast crossing to the $^1A_1$ state followed later by a crossing to the ground state at a conical intersection, which leads to the ring opening.

For this molecule the electronic structure was treated to balance accuracy with efficiency. The complete active space with perturbation theory (CASPT2) method, with 6 electrons in 6 orbitals and a 6-31G* basis set, was chosen as it is known that CASSCF incorrectly orders the key first and second excited states and CASPT2 corrects this. The CAS comprised the σ and σ^* orbitals of the C–C bond that breaks to form hexatriene from cyclohexadiene, and the 4 π-orbitals. A 3-state state-averaged calculation formed the basis for the CASPT2 correction. The extended multi-state multi-reference variant, XMS-CASPT2 [50], as implemented in Molpro2015 program [51] was used. Energies, gradients and the initial Hessians were taken from the CASPT2 calculations but the derivative couplings were calculated at the CASSCF level as these are not implemented at the CASPT2 level in Molpro2015. We note that derivative couplings have been implemented for XMS-CASPT2 in the BAGEL code [52] and used successfully in the TSH simulations of CHD by Poliak et al. [15]

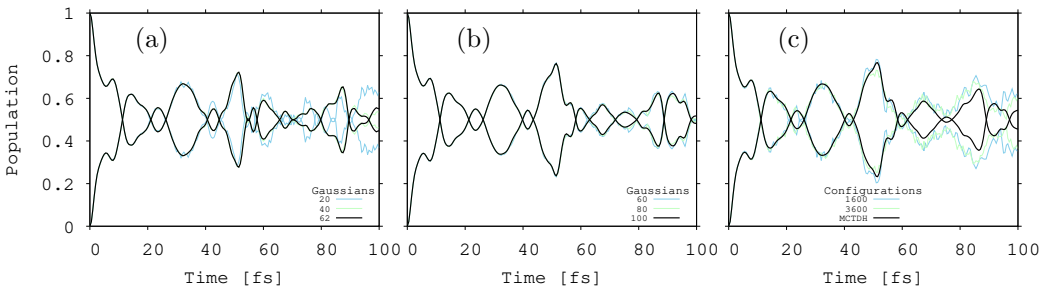

Figure 1. Diabatic state populations from vMCG simulations on the butatriene vibronic coupling model (a) 2D (b) 5D (c) 18D. Different numbers of GWP basis functions were used, as listed in the key for each plot. For (c) 18D, MM-vMCG is used to partition the SPF basis into 2 sets of 9D GWPs, and the key lists the total number of configurations used to describe the wavefunction.

The direct dynamics database was constructed calculating new structures if any atom deviated more than 0.25 Bohr from any structure in the database. As CASPT2 calculations can be unreliable close to a conical intersection, if the calculated surfaces are found to have an energy gap of less than 0.05 eV, the diabatic surfaces at the new point are obtained by extrapolation from the nearest point in the database rather than by transformation of the quantum chemistry adiabatic energies. Extrapolation of the diabatic surfaces are also used if the CASSCF reference fails to converge.

5. Analytical Surfaces: The Butatriene Model

The starting point for the investigation is to show the convergence properties of the vMCG method. In Fig. 1 the diabatic populations of two-dimensional, five-dimensional and 18-dimensional models obtained by MCTDH and vMCG calculations are shown. The 2D model includes the most important coupling mode with A_u symmetry (mode 5), and the most important totally symmetric A_g tuning mode (mode 14). The 5D model includes all five vibrational modes that couple linearly to the electronic states. This comprises all the totally symmetric (tuning) A_g modes (modes 8, 12, 14 and 15) and the coupling mode with A_u symmetry (mode 5), which is the torsional vibration. The 18D model is of the complete system. In all cases a fast population transfer between the diabatic states is seen. The 2D model is converged with 62 GWPs, the 5D model with 100 GWPs, while the 18D model was still not fully converged on the MCTDH result with 3600 configurations (60 GWPs for each particle). More details on the computational effort is given in the Supplementary Information.

TSH was then employed to study the dynamics of the butatriene cation using the same analytical surfaces as the MCTDH and vMCG calculations above. Up to 2001 trajectories were run in each case, and the populations do not change significantly after 401 trajectories. Both vMCG and MCTDH use a diabatic representation of the electronic wavefunction to allow numerically tractable simulations. In contrast, TSH calculations are run in the adiabatic picture. The state populations obtained in the two pictures are complementary: diabatic populations show the rate of transfer between the electronic configurations used to define the basis, while adiabatic populations show the rate of relaxation between the energy ordered states.

In order to compare the vMCG and MCTDH calculations with TSH, it is necessary to have populations in the same representation. Ideally adiabatic populations should be obtained from the full quantum dynamics methods to provide a benchmark. This, however, requires a non-trivial transformation as the adiabatic-diabatic transformation operator is only defined globally. To obtain adiabatic populations from MCTDH propagations in the past, Monte-Carlo integration of the transformation integral has been used. This, however, becomes unfeasible for more than 8-10 degrees of freedom as the occupied part of the huge configuration space is tiny, making the

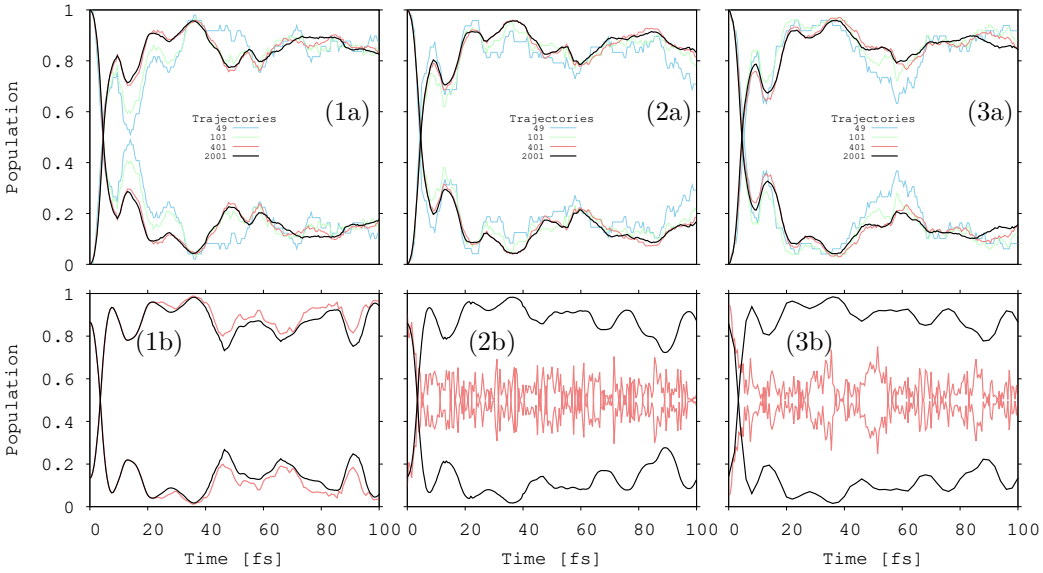

Figure 2.

Panel 1: Adiabatic electronic state populations for the butatriene model calculated (a) TSH (b) MCTDH. Panel 1, 2D model. Panel 2, 5D model. Panel 3, 18D model. For MCTDH, the populations calculated with TDDVR are in red and with the CDVR correction in black. For the 2D and 5D calculations the CDVR results are identical to the full solution.

sampling very inefficient. As a new approach used here, we use a time-dependent DVR (TDDVR) based on the single-particle function basis, including the correlated DVR (CDVR) extension known to be important for accurate integrals [53]. For vMCG, a saddle-point approximation was used, evaluating the integrals at the centres of the GWP basis functions. More details on how the adiabatic populations are obtained is in the Supplementary Information.

Figure 2 shows the adiabatic electronic state populations obtained from the TSH calculations, alongside the results from the MCTDH simulations. The adiabatic state populations for MCTDH on analytical PESs are comparable, albeit the details are different. Both TSH and MCTDH predict the crossing of adiabatic state populations at roughly the same time (ca. 5 fs), with the system then ending up almost entirely on the ground state. The main effect of including more modes is, as expected, a decrease in the strength of population recurrences at long times. For the MCTDH results, the TDDVR approximation fails badly for both the 5D and 18D models. In the latter cases, the adiabatic populations obtained are similar to the diabatic ones in Fig. 1 ending with roughly 50% of the population in each state. This is because TDDVR is simply unable to calculate good integrals due to the small number of points created relative to the space to be covered: for the 2D model there are 144 TDDVR points for a full grid of 442 points, while for the 18D model there are 1.3M TDDVR points, but the full grid is 4×10^{16} points.

6. Direct-Dynamics: Butatriene and Cyclohexadiene

Direct dynamics using both DD-vMCG and DD-TSH were run on the butatriene cation. As for the analytical model, simulations were made on 2D, 5D and 18D models, freezing the unwanted modes at their equilibrium geometry. For the first time the multi-mode vMCG formalism was used on the 18D system and shown to provide better convergence at much less computational expense.

Figure 3 shows the adiabatic populations from these runs. With the exception of the 18D DD-vMCG simulation, the qualitative behaviour is the same for all calculations, with a fast change in adiabatic state at around 10 fs. The 2D and 5D DD-vMCG calculations mirror closely the analytical

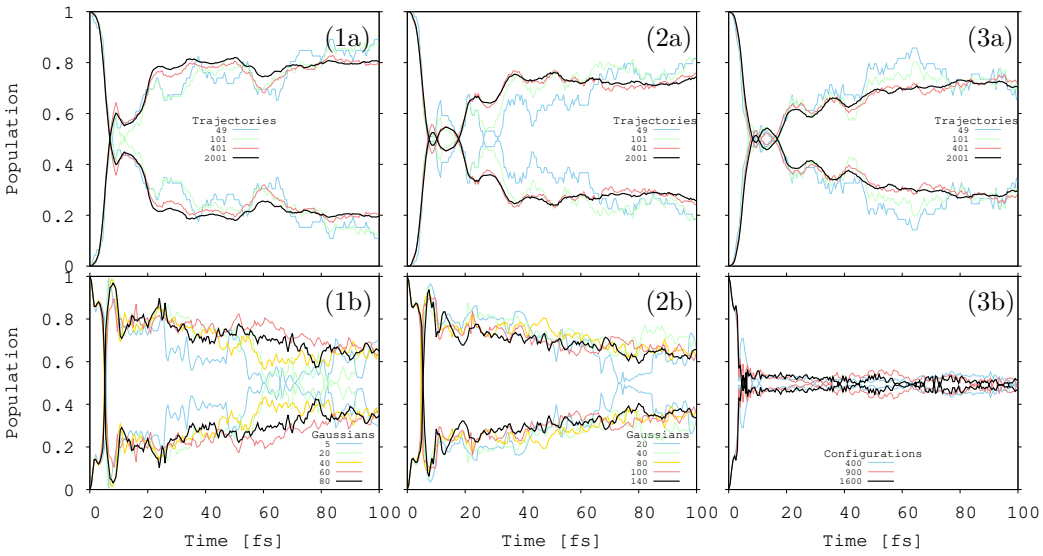

Figure 3. Adiabatic electronic state populations for the butatriene cation calculated using direct dynamics with potential surfaces at the CASSCF level and (a) TSH (b) DD-vMCG. Panel 1, 2D system. Panel 2, 5D system. Panel 3, 18D system. For (3b) DD-MM-vMCG is used to partition the SPF basis into 2 sets of 9D GWPs, and the key lists the total number of configurations used to describe the wavefunction. For DD-vMCG and DD-MM-vMCG, all diabatic-adiabatic transformations were calculated using saddle-point integration.

model during this crossing, whereas the TSH has a longer crossing time. At later times, there is also a difference seen with the DD-vMCG populations looking as though they are equilibrating, whereas the TSH remains on the lower state. As with the analytical model using the TDDVR approximation, it seems that obtaining integrals using only the centres of the GWPs in the saddle-point approximation obtains populations that are closer to the diabatic populations.

Finally, the populations from DD-vMCG and DD-TSH calculations on cyclohexadiene are shown in Fig. 4. A database with 1898 points was obtained from a series of full-dimensional (36D) calculations using 8, 16 and finally 32 GWPs, representing the potential surfaces required to describe the first 150 fs of dynamics. This database was then used for a simulation with a wavefunction partitioned into two 18D particles which used 32 GWPs for each. The partitioning was done on the basis of an analysis from the initial runs, determining the key vibrations, and these were put together in one particle. A DD-TSH simulation with 200 trajectories was also run on the surfaces provide by the database. A vertical excitation of the ground-state vibrational wavefunction in the harmonic approximation was modelled.

Both calculations show similar timescales for the population relaxation, with population initially crossing from S_1 to S_2 before relaxing to the S_0 state. As both crossings are sloped it is not surprising that the adiabatic and diabatic populations are more similar than in the case of butatriene. However, the marked similarity between two pictures for the DD-vMCG results indicates that again the saddle point scheme used is not able to produce a good result due to the small number of configurations. Further analysis of the dynamics needs to be performed in order to obtain detailed information as to when and how the state crossings occur. In addition to improving the diabatic-adiabatic transformation in vMCG calculations, a possible approach for this comparison would be the computation of the diabatic populations in TSH simulations. While ways for doing this have been proposed [41,54], a systematic implementation is not yet available.

A simple search through the database for regions where the surfaces become degenerate found two conical intersections. These are shown in Fig. 5 as cuts through the potential surfaces along linear vectors from the Franck-Condon point to the intersection. The crossing between S_1 and S_2 is close to the FC point and can be easily reached, as shown by the early population transfer.

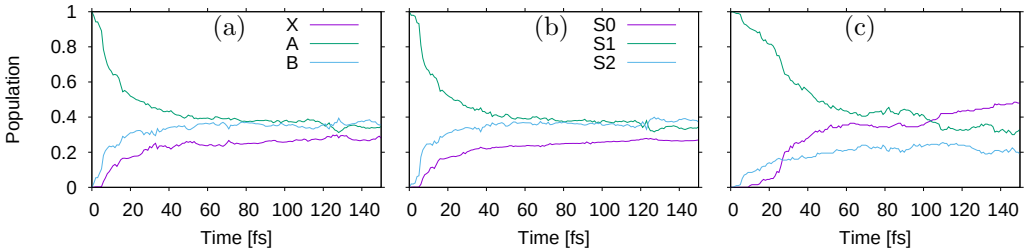

Figure 4. State populations from cyclohexadiene simulations starting on S_1. (a) DD-vMCG diabatic populations (b) DD-vMCG adiabatic populations (c) DD-TSH adiabatic populations

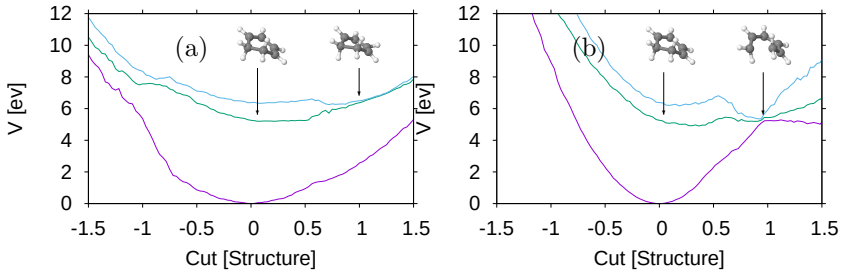

Figure 5. Cuts through the adiabatic surfaces from the quantum chemistry database collected during DD-vMCG simulations on cyclohexadiene. (a) From the Franck-Condon point to the S_1/S_2 intersection. (b) From the Franck-Condon point to the $S_1/S_2/S_3$ ring-opened intersection.

The second crossing looks like a 3-state intersection between all three states, hence is responsible for crossing to the ground-state. It is at a ring-opened geometry, in agreement to earlier studies, and can thus lead to hexatriene. While this intersection looks to be directly accessible from the FC point, it may not be accessed in the early stages of the dynamics as it requires the excitation of out-of-plane vibrations, none of which are activated directly by the initial photo-excitation. A small barrier is seen on the S_1 state, while a larger barrier on the S_2 surface can be observed. However, this feature may be indicative of a problem with the CASSCF calculations, as seen in recent DD-vMCG calculations on phenol which were solved by including higher lying states [55].

A final note can be made on computational effort. For these calculations the quantum chemistry is a major bottleneck. Each single point calculation of energies, gradients and derivative couplings took over 3 hours on the compute cluster used. If the DD-TSH calculations were run in the usual way with the electronic structure calculated at every step, the 200 trajectories would have required 300,000 calculations as the step size for the trajectories was 0.1 fs. The database filled by the DD-vMCG calculations, however, contains only 1898 structures. The use of the database and interpolation scheme thus saved a significant amount of computational effort by calculating points only as required. While the size of the database needed will be very molecule specific, depending on the range of motions seen during the dynamics. This saving will generally be the case as some regions, such as around the Franck-Condon point, are visited by many trajectories and effort is wasted recalculating similar structures.

7. Conclusion

The three methods for non-adiabatic dynamics presented here are complementary. For accurate simulations when an analytic potential surface is available MCTDH is the most efficient. vMCG provides a compact, trajectory-based representation of the wavefunction and converges much quicker than TSH. This makes it particularly suitable for generating potential surfaces using direct dynamics. TSH is able to provide adiabatic populations for large systems that are still not possible with either MCTDH or vMCG.

Further investigations are needed to provide deeper insight into the differences between the results from the 3 methods and how to best use them. The QUANTICS package provides a convenient platform for such investigations. In particular, the database generated during a direct dynamics simulation can be re-used in further calculations without having to re-run the quantum chemistry calculations. By using interpolation on a minimal number of points it also saves significant effort.

Non-adiabatic simulation methods are still under development but, as demonstrated here, they are presently able to provide information on medium sized molecules of varying complexity. As a result they provide a key tool in the understanding of photo-activated processes where the nuclear-electronic interactions must be treated at a quantum level.

Data Accessibility. The QUANTICS Package is opensource code, hosted on Gitlab and accessible by request to the corresponding author. The data from the simulations is likewise available on request.

Authors' Contributions. MS and ND wrote the Zagreb SH code. KES, CSS and GAW wrote the QUANTICS-Zagreb SH interface and relevant parts of DD-vMCG QUANTICS code. JC and GAW ran the calculations and drafted the manuscript. All authors read and approved the manuscript.

Competing Interests. The authors declare that they have no competing interests.

Funding. The QUANTICS-Zagreb SH interface was written with support from the European E-Cam project (www.e-cam2020.eu). CSS acknowledges the funding by the Spanish Ministry of Science and Innovation (Grant project Nr. FIS2017-83473-C2-P) and the COST Action CM1405 for the short term scientific mission visiting Prof. Nadja Doslic.

References

1. Curchod BFE, Martínez T. 2018 Ab initio nonadiabatic quantum molecular dynamics. *Chem. Rev.* **118**, 3305–3336.
2. Tannor DJ. 2007 *Introduction to quantum mechanics: a time-dependent perspective*. University Science Books.
3. Neufeld A. 2005 Statistical theory of nonadiabatic transitions. *J. Chem. Phys.* **122**, 164111.
4. Meyer HD, Gatti F, Worth GA. 2009 *Multidimensional quantum dynamics: MCTDH theory and applications*. John Wiley & Sons.
5. Tully JC. 1998 Mixed quantum-classical dynamics. *Faraday Discuss.* **110**, 407–419.
6. Richings GW, Polyak I, Spinlove KE, Worth GA, Burghardt I, Lasorne B. 2015 Quantum dynamics simulations using Gaussian wavepackets: the vMCG method. *Int. Rev. Phys. Chem.* **34**, 269–308.
7. Thompson DL. 1998 *Modern methods for multidimensional dynamics computations in chemistry*. World Scientific.
8. Tully JC. 1990 Molecular dynamics with electronic transitions. *J. Chem. Phys* **93**, 1061–1071.
9. Worth GA, Giri K, Richings GW, Burghardt I, Beck MH, Jäckle A, Meyer HD. 2021. Quantics package, version 2.0.
10. Worth G. 2020 Quantics: A general purpose package for quantum molecular dynamics simulations. *Comput. Phys. Commun.* **248**, 107040.

11. Cederbaum LS, Domcke W, Köppel H, von Niessen W. 1977 Strong vibronic coupling effects in ionization spectra: The "mystery band" of butatriene.
Chem. Phys. **26**, 169–177.
12. Cattarius C, Worth GA, Meyer HD, Cederbaum LS. 2001 All mode dynamics at the conical intersection of an octa-atomic molecules: Multi-configuration time-dependent Hartree (MCTDH) investigation on the butatriene cation.
J. Chem. Phys. **115**, 2088–2100.
13. Richings GW, Worth GA. 2015 A practical diabatisation scheme for use with the direct-dynamics variational multi-configuration Gaussian method.
J. Phys. Chem. A **119**, 12457–12470.
14. Arruda BC, Sension RJ. 2014 Ultrafast polyene dynamics: the ring opening of 1,3-cyclohexadiene derivatives.
Phys. Chem. Chem. Phys. **16**, 4439–4455.
15. Polyak I, Hutton L, Crespo-Otero R, Barbatti M, Knowles PJ. 2019 Ultrafast photoinduced dynamics of 1,3-cyclohexadiene using XMS-CASPT2 surface hopping.
J. Chem. Theor. and Comp. **15**, 3929–3940.
16. Beck MH, Jäckle A, Worth GA, Meyer HD. 2000 The multiconfiguration time-dependent Hartree method: A highly efficient algorithm for propagating wavepackets.
Phys. Rep. **324**, 1–105.
17. Worth GA, Burghardt I. 2003 Full quantum mechanical molecular dynamics using Gaussian wavepackets.
Chem. Phys. Lett. **368**, 502–508.
18. Tully JC. 2012 Perspective: Nonadiabatic dynamics theory.
J. Chem. Phys. **137**, 22A301.
19. Subotnik JE, Amber Jain A, Landry B, Petit A, Ouyang W, Bellonzi N. 2016 Understanding the surface hopping view of electronic transitions and decoherence.
Ann. Rev. Phys. Chem. **67**, 387–417.
20. Frenkel J. 1934 *Wave Mechanics*.
Oxford, U.K.: Clarendon Press.
21. Wang H, Thoss M. 2003 Multilayer formulation of the multiconfiguration time-dependent hartree theory.
J. Chem. Phys. **119**, 1289–1299.
22. Manthe U. 2008 A multilayer multiconfigurational time-dependent hartree approach for quantum dynamics on general potential energy surfaces.
J. Chem. Phys. **128**, 164116.
23. Burghardt I, Meyer HD, Cederbaum LS. 1999 Approaches to the approximate treatment of complex molecular systems by the multiconfiguration time-dependent Hartree method.
J. Chem. Phys. **111**, 2927–2938.
24. Heller EJ. 1981 Frozen Gaussians: A very simple semiclassical approximation.
J. Chem. Phys. **75**, 2923–2931.
25. Martínez TJ, Ben-Nun M, Levine RD. 1996 Multi-electronic-state molecular dynamics: A wave function approach with applications.
J. Phys. Chem. **100**, 7884–7895.
26. Ben-Nun M, Martínez TJ. 2002 *Ab Initio* quantum molecular dynamics.
Adv. Chem. Phys. **121**, 439–512.
27. Shalashilin DV, Child MS. 2004 The phase space ccs approach to quantum and semiclassical molecular dynamics for high-dimensional systems.
Chem. Phys. **304**, 103–120.
28. Shalashilin DV, Burghardt I. 2008 Gaussian-based techniques for quantum propagation from the time-dependent variational principle: Formulation in terms of trajectories of coupled classical and quantum variables.
J. Chem. Phys. **129**, 84104–84109.
29. Römer S, Ruckenbauer M, Burghardt I. 2013 Gaussian-based multiconfiguration time-dependent hartree: A two-layer approach. I. theory.
J. Chem. Phys. **138**, 64106–64113.
30. Di Maiolo F, Worth GA, Burghardt I. 2021 Multi-layer gaussian-based multi-configuration time-dependent hartree (ML-GMCTDH) simulations of ultrafast charge separation in a donor–acceptor complex.
J. Chem. Phys. **154**, 144106.

31. Messiah A. 1968.
Quantum mechanics john wiley & sons.
32. Subotnik JE, Shenvi N. 2011 Decoherence and surface hopping: When can averaging over initial conditions help capture the effects of wave packet separation?
J. Chem. Phys. **134**, 244114.
33. Jaeger HM, Fischer S, Prezhdo OV. 2012 Decoherence-induced surface hopping.
J. Chem. Phys. **137**, 22A545.
34. Granucci G, Persico M. 2007 Critical appraisal of the fewest switches algorithm for surface hopping.
J. Chem. Phys. **126**, 134114.
35. Vindel-Zandbergen P, Ibele LM, Ha JK, Min SK, Curchod BF, Maitra NT. 2021 A study of the decoherence correction derived from the exact factorization approach for non-adiabatic dynamics.
arXiv preprint arXiv:2104.04025 .
36. Martens CC. 2019 Classical and nonclassical effects in surface hopping methodology for simulating coupled electronic-nuclear dynamics.
Faraday Discuss. **221**, 449–477.
37. Herman MF. 1984 Nonadiabatic semiclassical scattering. i. analysis of generalized surface hopping procedures.
J. Chem. Phys. **81**, 754–763.
38. Pechukas P. 1969 Time-dependent semiclassical scattering theory. i. potential scattering.
Phys. Rev. **181**, 166.
39. Coker DF, Xiao L. 1995 Methods for molecular dynamics with nonadiabatic transitions.
J. Chem. Phys. **102**, 496–510.
40. Shu Y, Zhang L, Varga Z, Parker KA, Kanchanakungwankul S, Sun S, Truhlar DG. 2020 Conservation of angular momentum in direct nonadiabatic dynamics.
J. Phys. Chem. Lett. . **11**, 1135–1140.
41. Xie W, Sapunar M, Došlić N, Sala M, Domcke W. 2019 Assessing the performance of trajectory surface hopping methods: Ultrafast internal conversion in pyrazine.
J. Chem. Phys. **150**, 154119.
42. Meek GA, Levine BG. 2014 Evaluation of the time-derivative coupling for accurate electronic state transition probabilities from numerical simulations.
J. Phys. Chem. Lett. **5**, 2351–2356.
43. Jain A, Alguire E, Subotnik JE. 2016 An efficient, augmented surface hopping algorithm that includes decoherence for use in large-scale simulations.
J. Chem. Theory Comput. **12**, 5256–5268.
44. Granucci G, Persico M, Toniolo A. 2001 Direct semiclassical simulation of photochemical processes with semiempirical wave functions.
J. Chem. Phys. **114**, 10608.
45. Plasser F, Granucci G, Pittner J, Barbatti M, Persico M, Lischka H. 2012 Surface hopping dynamics using a locally diabatic formalism: charge transfer in the ethylene dimer cation and excited state dynamics in the 2-pyridone dimer.
J. Chem. Phys. **137**, 22A514.
46. Christopoulou G, Freibert A, Worth GA. 2021 Improved algorithm for the direct dynamics variational multi-configurational gaussian method.
J. Chem. Phys. **154**, 124127.
47. Köppel H, Domcke W, Cederbaum LS. 1984 Multimode molecular dynamics beyond the Born-Oppenheimer approximation.
Adv. Chem. Phys. **57**, 59–246.
48. Worth GA, Meyer HD, Köppel H, Cederbaum LS, Burghardt I. 2008 Using the mctdh wavepacket propagation method to describe multimode non-adiabatic dynamics.
Int. Rev. Phys. Chem. **27**, 569–606.
49. Frisch MJ, Trucks GW, Schlegel HB, Scuseria GE, Robb MA, Cheeseman JR, Scalmani G, Barone V, Petersson GA, Nakatsuji H, Li X, Caricato M, Marenich A, Bloino J, Janesko BG, Gomperts R, Mennucci B, Hratchian HP, Ortiz JV, Izmaylov AF, Sonnenberg JL, Williams-Young D, Ding F, Lipparini F, Egidi F, Goings J, Peng B, Petrone A, Henderson T, Ranasinghe D, Zakrzewski VG, Gao J, Rega N, Zheng G, Liang W, Hada M, Ehara M, Toyota K, Fukuda R, Hasegawa J, Ishida M, Nakajima T, Honda Y, Kitao O, Nakai H, Vreven T, Throssell

K, Montgomery Jr JA, Peralta JE, Ogliaro F, Bearpark M, Heyd JJ, Brothers E, Kudin KN, Staroverov VN, Keith T, Kobayashi R, Normand J, Raghavachari K, Rendell A, Burant JC, Iyengar SS, Tomasi J, Cossi M, Millam JM, Klene M, Adamo C, Cammi R, Ochterski JW, Martin RL, Morokuma K, Farkas O, Foresman JB, , Fox DJ. 2009.
Gaussian 09, revision a.02.

50. Shiozaki T, Győrffy W, Celani P, Werner HJ. 2011 Communication: Extended multi-state complete active space second-order perturbation theory: Energy and nuclear gradients.
J. Chem. Phys. **135**, 081106.
51. Werner HJ, Knowles PJ, Knizia G, Manby FR, Schütz M, Celani P, Györffy W, Kats D, Korona T, Lindh R, Mitrushenkov A, Rauhut G, Shamasundar KR, Adler TB, Amos RD, Bernhardsson A, Berning A, Cooper DL, Deegan MJO, Dobbyn AJ, Eckert F, Goll E, Hampel C, Hesselmann A, Hetzer G, Hrenar T, Jansen G, Köppl C, Liu Y, Lloyd AW, Mata RA, May AJ, McNicholas SJ, Meyer W, Mura ME, Nicklass A, O'Neill DP, Palmieri P, Peng D, Pflüger K, Pitzer R, Reiher M, Shiozaki T, Stoll H, Stone AJ, Tarroni R, Thorsteinsson T, Wang M. 2015.
Molpro, version 2015.1, a package of ab initio programs.
52. Shiozaki T. 2018 BAGEL : Brilliantly advanced general electronic-structure library.
WIREs Comp. Mol. Sci. **8**, e1331.
53. Manthe U. 1996 A time-dependent discrete variable representation for (multiconfiguration) hartree methods.
J. Chem. Phys. **105**, 6989–6994.
54. Piteša T, Sapunar M, Ponzi A, Gelin MF, Došlić N, Domcke W, Decleva P. 2021 Combined surface-hopping, dyson orbital, and b-spline approach for the computation of time-resolved photoelectron spectroscopy signals: The internal conversion in pyrazine.
J. Chem. Theory and Comput. **17**, 5098–5109.
55. Christopoulou G, Tran T, Worth GA. 2021 Direct nonadiabatic quantum dynamics simulations of the photodissociation of phenol.
Phys. Chem. Chem. Phys. **xxx**, xxx.
Submitted